Proposed Mechanism of Antibacterial Action of Chemically Modified Apatite for Reduced Bone Infection

P. N. Lim,[†] L. Chang,[†] B. Y. Tay,[‡] V. Guneta,[§] C. Choong,[§] B. Ho,[‖] and E. S. Thian*,[†]

[†]Department of Mechanical Engineering, National University of Singapore, 9 Engineering Drive 1, Singapore 117 576, Singapore

[‡]Singapore Institute of Manufacturing Technology, 71 Nanyang Drive, Singapore 638 075, Singapore
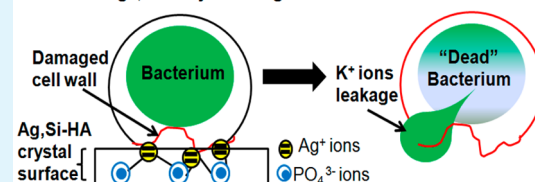
[§]School of Materials Science and Engineering, Nanyang Technology University, 50 Nanyang Avenue, Singapore 639 798, Singapore

[‖]Department of Microbiology, Yong Loo Lin School of Medicine, National University of Singapore, 5 Science Drive 2, Singapore 119 757, Singapore

ABSTRACT: Surface-bound silver ions were demonstrated to be responsible for the antibacterial action of silver, silicon-containing hydroxyapatite (Ag,Si-HA). X-ray photoelectron spectroscopy, transmission electron microscopy, and induced coupled plasma spectroscopy results suggested that silver ions in the crystal structure diffused toward the crystal surface of Ag,Si-HA, and interacted with adherent *Staphylococcus aureus* bacteria, thus damaging the cell wall and inducing leakage of potassium ions. All these steps constitute the mechanism of antibacterial action for Ag,Si-HA. Consequently, Ag,Si-HA gave rise to

Surface-bound Ag+ ions of Ag,Si-HA damage cell wall, and induce K+ ions leakage, thereby resulting in the death of bacterium

a 7-log reduction of the adherent bacteria as compared to HA and Si-HA at 168 h. Silicon in Ag,Si-HA helped to mitigate the reduced effect of bone differentiation in Ag-HA as shown in the alkaline phosphatase, type I collagen and osteocalcin results, promoting enhanced biological response, without compromising the antibacterial property. On the whole, Ag,Si-HA containing an optimized content of 0.5 wt % silver and 0.7 wt % silicon provides antibacterial properties and enhanced biological response.

KEYWORDS: antibacterial, apatite, silicon, silver, stem cell

1. INTRODUCTION

Bioactivity of a biomaterial plays an integral role for bone regeneration. During this process, optimal healing of the defect region relies heavily upon the prevention of bacterial infection following implant placement. Each year, implant-related infection affects about 2.6 million American patients and causes about 90 000 deaths during orthopedic surgeries.[1] Implant-related infection is a feared complication, which needs to be monitored closely after implantation. As in other medical intervention approaches, the insertion of medical prostheses such as a hydroxyapatite (HA)-based bone graft poses as a site of weakness for the host defense, making it susceptible to implant-related infections.

In order to encounter implant-related infection, incorporation of silver into HA (Ag-HA) has emerged as a potential approach. Silver is an excellent antimicrobial agent[2] and can be incorporated into the HA structure via ion exchange.[3] The antibacterial effect of Ag-HA against the bacteria in the medium was suggested to be dependent on the release of silver ions.[4−7] However, release of the silver ions was not easily controlled and tended to result in abrupt release of silver ions, leading to issues such as local toxicity and short-term antibacterial property.[4−7] Therefore, mechanism of antibacterial action dependent on released silver ion from Ag-HA may not be favorable for an effective antibacterial effect. An interesting observation was noted in our recent study with effective inhibition of bacterial growth on Ag-HA, despite detecting minimum released silver

ions,[8] and this observation was not reported in the literature. This initial finding signaled that the surface-bound silver ions of Ag-HA might be responsible for the antibacterial action, inhibiting the growth of adherent bacteria and bacteria in the test medium. The inhibition of surface bacterial colonization is crucial for the prevention of a biofilm. Surface-bound silver ions would be a good mode for the mechanism of antibacterial action of Ag-HA. However, its role on the mechanism of the antibacterial action remains elusive.

Although, antibacterial properties were created with the incorporation of silver, the biocompatibility of Ag-HA was compromised. Adhesion of mammalian cells was demonstrated to decrease with the increase of silver content in Ag-HA.[6] Similarly, the cytotoxicity of Ag-HA also increased with increasing silver content, as indicated by the increasing hemolysis ratio.[4,9] With a higher hemolysis ratio, there will be more breakage of the membrane of the red blood cell, leading to cell death. An approach of improving the osseointegration rate of HA is to adjust its chemical composition closer to that of the natural bone mineral through incorporation of similar ions such as silicon. Over the years, the incorporation of silicon into HA (Si-HA) has shown to have the potential to increase the rate of bone apposition on HA implants significantly.[10−13]

Thus, to improve the biocompatibility of Ag-HA, silicon was incorporated into Ag-HA containing 0.2 wt % silver, which was reported in our recent study.[14] Hence, it is the interest of this study to propose the mechanism for the antibacterial action of surface-bound silver in Ag,Si-HA. In addition, this study investigates the effect of silicon in influencing the biological response of Ag,Si-HA despite increasing the silver content to 0.5 wt %.

2. MATERIALS AND METHODS

2.1. Ag,Si-HA Disc. Ag,Si-HA was synthesized via an aqueous reaction between 0.4925 M calcium hydroxide (VWR) containing 0.0075 M silver nitrate (Merck) and 0.284 M orthophosphoric acid (Merck) containing 0.016 M tetraethyl orthosilicate (TEOS) (Sigma−Aldrich) at 25 °C. The pH of the mixture was adjusted to above 10.5 by the addition of aqueous ammonia (VWR). Stirring was maintained for 16 h, and the precipitate was then aged for 2 weeks before washing with distilled water. More details of the method are described in our previous study.[15] Similarly, HA was synthesized based on the same technique via an aqueous precipitation reaction between 0.5 M calcium hydroxide and 0.3 M orthophosphoric acid. Ag-HA was synthesized by the reaction between 0.4925 M calcium hydroxide containing 0.0075 M silver nitrate and 0.3 M orthophosphoric acid while Si-HA was synthesized by the reaction between 0.5 M calcium hydroxide and 0.284 M orthophosphoric acid containing 0.016 M TEOS. Phase-pure HA, Ag-HA, and Si-HA discs of almost similar morphology and crystallinity with Ag,Si-HA were used as controls for the antibacterial and biocompatibility assessments. Each sample was compacted uniaxially into ⌀12 mm discs before dry heating at 600 °C for 2 h in air for antibacterial and biocompatibility assessments.

The physicochemical properties of the dry-heated Ag,Si-HA disc were examined. Approximately 0.5 wt % silver and 0.7 wt % silicon were detected using X-ray fluorescence in the Ag,Si-HA disc used in this study. These were the optimized contents of silver and silicon incorporated in apatite as reported by Lim et al.[8] and Hing et al.,[16] respectively. A phase-pure apatite was produced for Ag,Si-HA in the X-ray diffraction patterns,[17] along with the phosphate, hydroxyl, and silicate functional groups in the Fourier transform IR spectra.[14] The incorporation of silver and silicon was further confirmed with the expansion of the lattice parameters and unit cell volume (Table 1). Therefore, it clearly demonstrated that silver and silicon were structurally incorporated into HA to form a single phase rather than existing as a second phase with HA.

Table 1. Structural Parameters Obtained from Lattice Refinement[a]

| sample	a (nm)	c (nm)	unit cell volume (nm^3)
HA	0.9410 (0.0004)	0.6886 (0.0004)	0.5280
Ag,Si-HA	0.9421 (0.0003)	0.6899 (0.0004)	0.5303

[a]Errors are ± standard errors of the mean, with the values in parentheses.

2.2. Surface Composition of the Ag,Si-HA Disc. The surface compositions of dry-heated Ag,Si-HA discs that were immersed in distilled water at days 1, 3, 5, and 7 were measured by X-ray photoelectron spectroscopy (XPS; Kratos AXIS Ultra DLD spectrometer) with an Al Kα radiation (1486.71 eV) at a constant dwell time of 100 ms and a pass energy of 40 eV. The anode voltage was 15 kV, and the anode current was 10 mA. The pressure in the analysis chamber was maintained at 7.0×10^{-6} Pa or lower during each measurement. The core-level signals were obtained at a photoelectron takeoff angle of 90° (with respect to the sample surface). All binding energies (BEs) were referenced to the C 1s hydrocarbon peak at 285 eV. A survey spectrum between −5 and 1100 eV was recorded. In the peak synthesis, the line width (full width at half-maximum, fwhm) of the Gaussian peaks was maintained constant for all components in a

particular spectrum. Surface elemental components were determined from peak area ratios corrected with the experimentally determined sensitivity factors and were reliable to 10%. Narrow scan of the Ag 3d$_{5/2}$ peak was deconvoluted through the XPS peak fit software, using mixed Gaussian−Lorentzian functions, the nonlinear squares fitting algorithm, and Shirley-type background subtraction.

2.3. Antibacterial Assessment of the Ag,Si-HA Disc. The antibacterial effect on the growth of *Staphylococcus aureus* (ATCC 25923) was examined using a log reduction assay. Each disc was immersed in 2 mL of peptone water containing 1.5×10^7 cells/mL in a 24-well plate and incubated at 37 °C at various time points of 6, 12, 18, 24, 72, 120, and 168 h. At the end of each incubation period, the disc was removed from the test solution and gently rinsed three times with phosphate-buffered saline (1X PBS, pH = 7.4) solution. After washing, the disc was transferred into a new tube containing 5 mL of peptone water and vortexed vigorously for 60 s to remove any bacteria adhering on the surface of the disc. A 10-fold dilution was carried out on the vortexed solution. For each time point, 25 μL of each diluted vortexed solution was plated onto a tryptone soya agar (Oxoid) in duplicate. The plates were incubated at 37 °C for another 24 h to allow enumeration of viable bacteria. The log reduction assay was also conducted for HA, Ag-HA, and Si-HA discs.

The antibacterial action of the surface-bound silver ions of the Ag,Si-HA disc was examined in another separate antibacterial assessment. An insert with membrane pore size of 0.4 μm was placed in the well (Figure 1) to prevent samples from coming in contact with
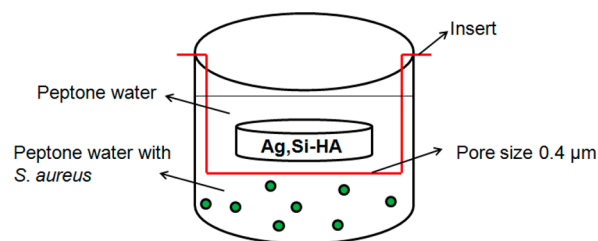
Figure 1. Schematic drawing of the setup of the inset in the well plate.

S. aureus (3×10^7 cells/mL). A similar setup was used for untreated bacteria and the HA disc. The 24-well plate was incubated at 37 °C for 24 h, after which 100 μL of the test solution was removed from each of the wells in the 24-well plate. The concentration of the test solution was serially diluted. An aliquot of 25 μL of the latter of various dilutions was added onto a tryptone soya agar in duplicate and incubated at 37 °C for another 24 h to allow enumeration of viable bacterial. Two sets of replicates were performed, and the mean value was calculated. The growth of *S. aureus* in the test solution of Ag,Si-HA without the placement of insert was also determined and compared in the study.

2.4. Characterization on the Effect of *S. aureus* Treated with Ag,Si-HA. *2.4.1. Gram Staining.* Gram staining was carried out to inspect the peptidoglycan layer of the cell wall of *S. aureus* after interacting with HA and Ag,Si-HA discs. *S. aureus* at a concentration of 10^7 CFU/mL was incubated at 37 °C for 6 h. Similarly, the bacteria was treated with HA and Ag,Si-HA discs at 37 °C for 6 h, following which an aliquot of 30 μL of the test solution of each sample (untreated bacteria, treated with HA and Ag,Si-HA) was smeared onto a glass slide, fixed by heating at 80 °C, and washed. Primary stain (crystal violet) was added onto the heat-fixed smear of the bacteria culture for 1 min, washed, and dried. Iodine was then added onto the heat-fixed smear of the bacteria smear for 1 min, and it was washed and dried before 95% ethanol was added to decolorize the stain for 10 s, followed by washing and drying. Lastly, it was counterstained with carbol fuchsin for 1 min, washed, and dried for optical microscope observation.

2.4.2. Transmission Electron Microscopy (TEM). TEM was carried out to inspect the morphological structural changes of *S. aureus* following interaction with Ag,Si-HA disc. *S. aureus* at a concentration of 10^7 CFU/mL was incubated at 37 °C for 6 h. Similarly, the bacteria

was treated with HA and Ag,Si-HA discs at 37 °C for 6 h. Bacterial cell pellets were then obtained by centrifuging at 5200g for 30 min and washing twice with 1X PBS (pH = 7.4) solution. The bacteria cell pellet of each sample (untreated bacteria, treated with HA and Ag,Si-HA) was fixed in 2.5% glutaraldehyde at 4 °C overnight. The glutaraldehyde-fixed samples were then washed and postfixed in 1% osmium tetroxide for 1 h at 24 °C. The postfixed samples were first encapsulated in gelatin and fixed with 2.5% glutaraldehyde for 1 h at 4 °C. The gelatin-fixed samples were washed, trimmed into small blocks of 1−2 mm³, and dehydrated through a series of ethanol and acetone. The small blocks of gelatin-fixed samples were further infiltrated with a solution of acetone and Araldite resin, ratio 1:1 for 1 h and then 1:6 overnight. Subsequently, the small blocks of gelatin-fixed samples were infiltrated in Araldite resin with increasing temperature and finally embedded with Araldite and polymerized at 60 °C for 24 h. Ultrathin sections (approximately 0.1 μm thickness) were cut with a glass knife using an ultramicrotome (Lecia ultracut) and then mounted on copper grids. The ultrathin sections were then stained with lead citrate for TEM (JEOL) observation.

2.4.3. Inductively Coupled Plasma (ICP) Spectroscopy. ICP spectroscopy (PerkinElmer dual-view optima 5300 DV ICP-OES system) was used to measure the amount of potassium ions leaking from untreated *S. aureus* and *S. aureus* treated with HA and Ag,Si-HA in test solution for 6 h. HA and Ag,Si-HA discs were immersed in 2 mL of peptone water containing 2 × 10⁷ cells/mL in a 24-well plate, and incubated at 37 °C for 6 h. At 6 h, 1 mL of the test solution of each sample (untreated bacteria, treated with HA and Ag,Si-HA) was centrifuged, and the supernatant was tested by ICP spectroscopy to measure the leakage of potassium ions from the inactive bacteria. Two replicates were measured, and the mean value was calculated.

2.5. Biocompatibility Assessment of the Ag,Si-HA Disc. Biological response was evaluated using human adipose-derived mesenchymal stem cells (hASCs) isolated from human adipose tissue lipoaspirate (Invitrogen, StemPro Human Adipose-Derived Stem Cell Kit, Passage 2). hASCs were used as they could potentially undergo multilineage differentiation along mesenchymal lineages: adipogensis, chondrogenesis, osteogenesis, and myogenesis. They are patient-specific and easier to isolate from adipose tissue than bone marrow mesenchymal stem cells (MSCs). hASCs have a higher stem proliferation rate than bone marrow MSCs.[18] hASCs were thawed, cultured, and maintained in MesenPRO RS medium for 4−5 passages and subsequently used for experiments. Each HA, Ag-HA, Si-HA, and Ag,Si-HA disc was sterilized by UV exposure for 30 min preceded by extensive washing with 1X PBS (pH = 7.4) solution. A total of 2 × 10⁴ cells were then seeded on each sterilized disc before incubating at 37 °C in a humidified atmosphere of 95% air and 5% carbon dioxide. After 7 days, the growth media was changed to osteogenic inductive media (Invitrogen, StemPro Osteogenesis Differentiation Kit), which is the growth medium supplemented with 10 mM β-glycerolphosphate, 100 μM ascorbic acid, and 10⁻⁸ M dexamethasone. Media changes were performed every alternate day.

2.5.1. Cell Proliferation. Cell proliferation was measured using the alamarBlue assay (Invitrogen). Cells cultured on the discs (HA, Ag-HA, Si-HA, and Ag,Si-HA) were incubated with 0.5 mL of 10% alamarBlue reagent in serum free media for 4 h in a 5% CO₂ environment at 37 °C on days 1, 3, 5, and 7. After 4 h, the fluorescence density was measured at an excitation wavelength of 570 nm, with an emission wavelength of 580 nm using the microplate reader (SpectraMax Gemini microplate, Molecular Devices). Cell numbers were calculated by correlating the fluorescence emission with known quantities of cells.

2.5.2. Cell Morphology. On days 5, 14 and 21, the adherent hASCs on discs were fixed with 0.2% glutaraldehyde, dehydrated through a series of ethanol concentrations (25%, 50%, 75%, 95%, 100% (v/v) in distilled water), vacuum-dried, and coated with a layer of gold before viewing by scanning electron microscopy (SEM).

2.5.3. Alkaline Phosphatase (ALP), Type I Collagen (COL I), Osteocalcin (OCN) Expression. ALP activity of hASCs cultured on discs was measured using an ALP fluorescent assay (ab83371, abcam) on days 14, 21, and 28. The cells underwent lyses by three cycles of

freeze thaw, and subsequently, 50 μL of 0.2% Nonidet P40 (Sigma−Aldrich) substitute was added to each sample. An aliquot of 10 μL of TRIS/bovine serum albumin and 100 μL of 4-methyl-umbelliferyl phosphate (4-MUP) working solution were added to each lysate and incubated at 37 °C for 40 min. To the mixture, 100 μL of 0.6 M sodium carbonate was added to each well to stop the reaction, and fluorescence at 360/450 nm was measured using a 96-well plate microplate reader (SpectraMax Gemini microplate, Molecular Devices). ALP reacted with 4-MUP to form 4-methyl-umbelliferone (4-MU), and the rate of the 4-MU formation was directly proportional to the level of ALP. Thus, ALP can be determined by measuring the rate of 4-MU formation. The 4-MU value was obtained by cross-referencing to a standard calibration curve of 4-MU count against fluorescence done at the beginning of the study to obtain the 4-MU count over a range 0−1000 pmol of 4-MU. Finally, ALP activity was calculated using eq 1 obtained from the Alkaline Phosphatase Assay Kit (ab83371, abcam):

$$\text{ALP activity} = A/V/T \ \ (\text{mU/mL})$$

$$A = \text{amount of 4-MU generated by samples (in nmol)}$$

$$V = \text{volume of sample in assay well (0.05 mL)}$$

$$T = \text{reaction time (40 min)} \tag{1}$$

ALP results were then normalized to cell number by dividing the ALP activity with the cell number obtained from the alamarBlue assay at days 14, 21, and 28.

COL I expression of hASCs cultured on samples was determined by enzyme immunoassay (Metra CICP EIA kit, Quidel) on days 14, 21, and 28. For analysis, the culture medium was first diluted with assay buffer at a ratio of 1:3. An aliquot of 100 μL of sample was then added to each well, and the sample was incubated at 25 °C for 2 h. The wells were washed three times with 300 μL of wash buffer before adding 100 μL of rabbit anti-CICP, and the sample was incubated at 25 °C for 50 min. The wells were washed again three times with the wash buffer. Next, 100 μL of reconstituted enzyme conjugate was added, and the sample was incubated at 25 °C for 50 min. A final wash was performed before 100 μL of working substrate solution was added, and the sample was incubated for 30 min. Finally, 50 μL of stop solution was added, and fluorescence was read at 405 nm. The CICP assay is a sandwich enzyme immunoassay in a microplate format utilizing a monoclonal anti-CICP antibody coated on the plate, a rabbit anti-CICP antiserum, a goat antirabbit ALP conjugate, and a pNPP substrate to quantify COL I. All the readings were first corrected by the mean of the blank group measurements. The standard data points were plotted, where y is the corrected optical measurement and x is the concentration, and a four parameter logistic fit was made through these points to determine A, B, C, and D coefficients in eq 2:[19]

$$y = (A - D)/(1 + (x/c)^B) + D \tag{2}$$

The COL I results of HA, Ag-HA, Si-HA, and Ag,Si-HA were determined from the fit. The COL I results of the samples should fall within the range of the determined upper and lower asymptotes of the fit (A and D coefficients). COL I results were then normalized to the cell number by dividing the COL I expression with the cell number obtained from the alamarBlue assay at days 14, 21, and 28.

OCN expression of hASCs cultured on samples was measured by an enzyme immunoassay (Metra Osteocalcin ELISA kit, Quidel) on days 14, 21, and 28. First, 25 μL of cell medium and 125 μL of antiosteocalcin antibody were added to each well before incubating at 25 °C for 2 h. The wells were then washed three times with 300 μL of wash buffer. Following that, 150 μL of reconstituted enzyme conjugate was added, and the sample was incubated at 25 °C for 1 h. The wells were again washed three times before 50 μL of working substrate solution was added, and the sample was incubated at 25 °C for 35 min. Finally, 50 μL of stop solution was added, and fluorescence was read at 405 nm. OCN assay used OCN coated strips, a mouse anti-OCN antibody, an antimouse lgG-ALP conjugate, and a pNPP substrate to quantify OCN in serum. The OCN results were also determined using
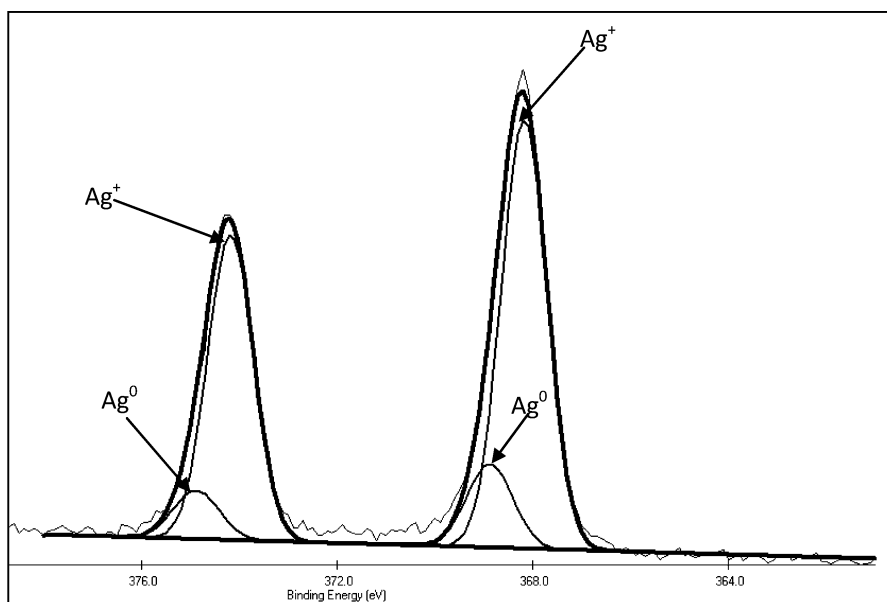
Figure 2. XPS spectra of the Ag $3d_{5/2}$ region on the surface of Ag,Si-HA disc immersed for 7 days.

the four parameter logistic fit, which was reported in eq 2. OCN results were then normalized to the cell number by dividing the OCN expression with the cell number obtained from the alamarBlue assay at days 14, 21, and 28.

2.6. Statistical Analysis. A two-way analysis of variance, followed by Turkey's posthoc testing was used to determine any significant differences existing between the mean values of the experimental groups for the log reduction assay, alamarblue, ALP, COL I, and OCN. A difference between groups was considered to be significant at $p < 0.05$. Two replicates were measured for the log reduction assay with two independent repeats, and the mean value was calculated. Five replicates were measured for alamarblue with two independent repeats, and the mean value was calculated. Four replicates were measured for the ALP, COL I, and OCN assays with two independent repeats, and the mean value was calculated.

3. RESULTS

3.1. Content of Surface-Bound and Released Silver Ions. Figure 2 illustrates the oxidation states of silver on the surface of the Ag,Si-HA disc, which was immersed in distilled water for 7 days. The peaks were fitted by using two doublets with the BE and fwhm reported in the literature data.[20] The silver $3d_{5/2}$ signals at 368.0 ± 0.3 eV and 374.1 ± 0.2 eV were related to the silver ion (Ag$^+$) while signals at 368.7 ± 0.2 eV and 374.9 ± 0.3 eV corresponded to metallic silver (Ag^0). Figure 3 shows the amount of silver (with respect to the number of elements measured) on the surface of Ag,Si-HA and the amount of released silver ions from Ag,Si-HA. It was observed that the amount of silver ions on the surface of Ag,Si-HA increased with the immersion period. On the other hand, the amount of released silver ions from Ag,Si-HA was very minimal (0.00004 wt %), and the total amount of released silver ions at day 7 was less than 0.0002 wt % silver in Ag,Si-HA.

3.2. Antibacterial Assessment of the Ag,Si-HA Disc. The viability of adherent *S. aureus* on HA and all substituted apatites discs were investigated using the log reduction assay for a period up to 168 h (Figure 4). At 6 h, adherent *S. aureus* on the HA disc grew steadily from a population of approximately 1 × 10^7 CFU/mL to a population of 3 × 10^7 CFU/mL while adherent *S. aureus* on the Si-HA disc maintained its population around 7 × 10^7 CFU/mL over a period of 168 h. On the other
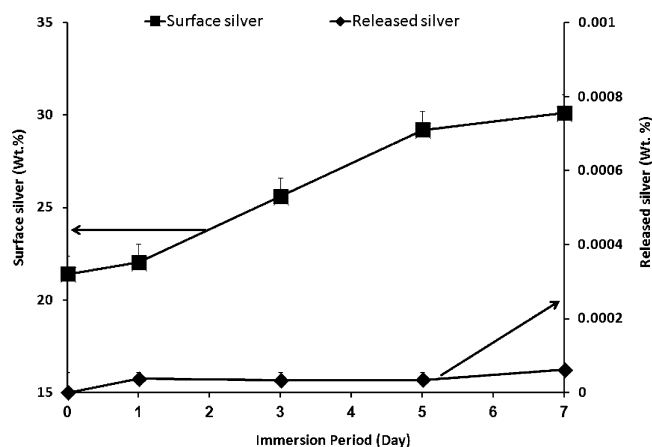

Figure 3. Amount of surface-bound silver ions and released silver ions of Ag,Si-HA with immersion period (bars represent standard error of the mean).
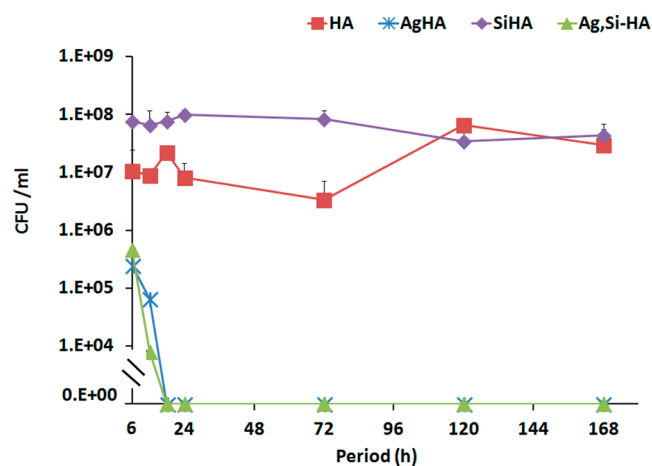

Figure 4. Log reduction assay of adherent *S. aureus* on HA, Ag-HA, Si-HA, and Ag,Si-HA discs (bars represent standard error of the mean).

hand, 4×10^5 CFU/mL of adherent *S. aureus* was detected on Ag-HA and Ag,Si-HA discs at 6 h. The number of adherent *S. aureus* on Ag-HA and Ag,Si-HA discs was further reduced to 6×10^4 CFU/mL and 8×10^3 CFU/mL at 12 h, respectively. By 18 h, the number of adherent *S. aureus* on both samples was reduced to zero, and this remained until 168 h. Overall, a 7-log reduction of the adherent *S. aureus* was observed for Ag,Si-HA and Ag-HA as compared to HA and Si-HA over a culture period of 168 h.

3.3. Surface-Bound Silver Ions of Ag,Si-HA for Antibacterial Action.

On the basis of the increasing silver content on the surface of the Ag,Si-HA disc and the significant reduction of adherent bacteria on the Ag,Si-HA disc reported in the present study, it can be hypothesized that the surface-bound silver ions of Ag,Si-HA were responsible for the antibacterial action. Having cultured for 24 h on insert, untreated *S. aureus* (without the Ag,Si-HA disc) in the test solution grew from an average starting population of 3×10^7 to 3×10^8 CFU/mL (Figure 5). This growing trend was also observed in the test
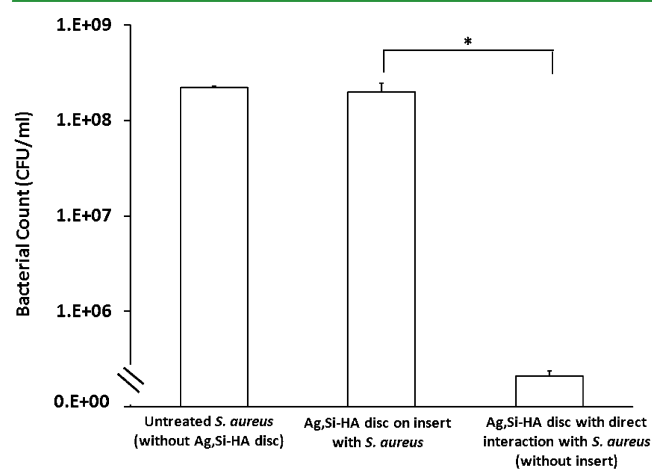

Figure 5. Log reduction assays of the test solution in untreated *S. aureus* (without the Ag,Si-HA disc), the Ag,Si-HA disc on insert with *S. aureus*, and the Ag,Si-HA disc with direct interaction with *S. aureus* (without insert) incubated for 24 h (bars represent standard error of the mean, * $p < 0.05$).

solution of the Ag,Si-HA disc on insert with *S. aureus*. On the other hand, with the absence of insert, the Ag,Si-HA disc with direct interaction with *S. aureus* in the test solution decreased from 3×10^7 to 2×10^5 CFU/mL.

3.4. Effect on *S. aureus* Treated with Ag,Si-HA.

The damage of the peptidoglycan layer of *S. aureus* treated with Ag,Si-HA was examined by Gram staining. Figure 6 shows that untreated *S. aureus* and *S. aureus* treated with HA were stained purple due to the thick peptidoglycan layer of the cell wall. On the other hand, it was observed that the majority of *S. aureus* that were treated with Ag,Si-HA stained pink, with few stained purple. The damage of the membrane of *S. aureus* was further examined under TEM.

Figure 7 shows the morphology of untreated *S. aureus* and morphological changes of *S. aureus* treated with HA and Ag,Si-HA for 6 h. Untreated *S. aureus* and *S. aureus* treated with HA retained their coccus morphology (600 nm in diameter), with a homogeneous electron density in the cytoplasm (Figures 7a, b). Their cell walls and membranes were intact, exhibiting a well-preserved peptidoglycan layer and cytoplasmic membrane.
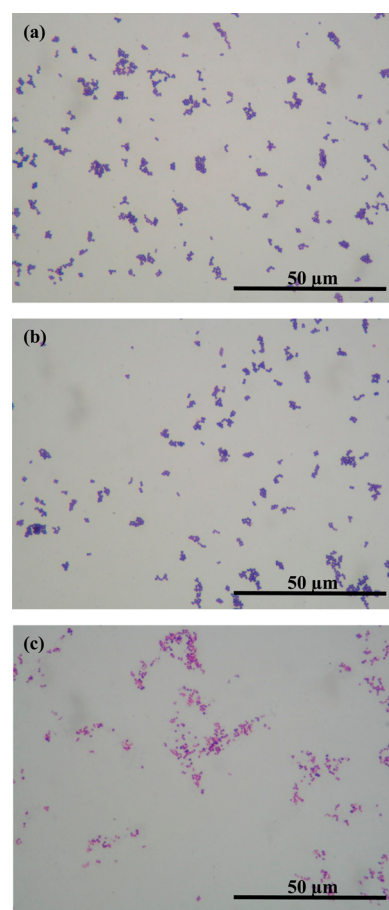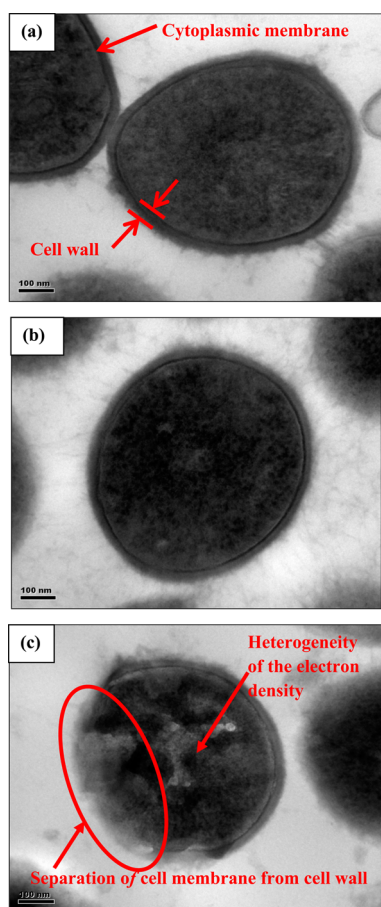

Figure 6. Gram staining of (a) untreated *S. aureus*, (b) *S. aureus* treated with HA, and (c) *S. aureus* treated with Ag,Si-HA for 6 h.

In contrast, noticeable morphological changes were observed in *S. aureus* treated with Ag,Si-HA for 6 h (Figure 7c). An electron-light region appeared, indicating heterogeneity of the electron density in the cytoplasm after being treated with Ag,Si-HA. The cell wall and the membrane of *S. aureus* were ruptured, displaying an aberrant morphology. In addition, detachment of the cytoplasm membrane from the cell wall could be discerned.

Changes in the bacterial membranous permeability and destruction of the cell membrane could cause enzymes such as potassium ions in the cell to leak.[21] Figure 8 shows the leakage of potassium ions from untreated *S. aureus* and *S. aureus* treated with HA and Ag,Si-HA for 6 h. There was a significantly higher amount of potassium ions leakage ($p < 0.05$) in the damaged cell membrane of *S. aureus* treated with Ag,Si-HA as compared to HA.

3.5. Biocompatibility Assessment of the Ag,Si-HA Disc.

The cell proliferation of hASCs on HA and substituted apatite is presented in Figure 9. The alamarBlue assay demonstrated a continuous cell growth for HA and Ag-HA from days 1 to 7. A continuous cell growth for Ag,Si-HA and Si-HA was also observed from days 1 to 3, but cell growth tended to level off and reached a plateau for Si-HA and Ag,Si-HA from days 3 to 5. The slow cell growth from days 5 to 7 indicated that hASCs on Si-HA and Ag,Si-HA might have reached the confluent stage.

SEM micrographs in Figures 10−12 illustrate the cell morphology cultured on HA and all substituted apatites, for
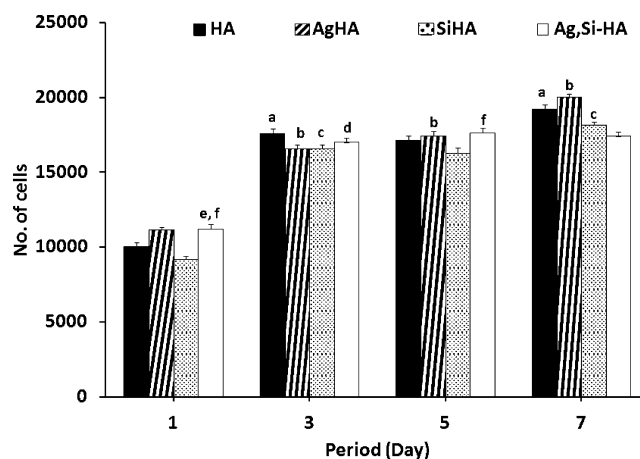
Figure 7. Morphological changes in *S. aureus* as observed under TEM. (a) Untreated *S. aureus*, (b) *S. aureus* treated with HA, and (c) *S. aureus* treated with Ag,Si-HA.
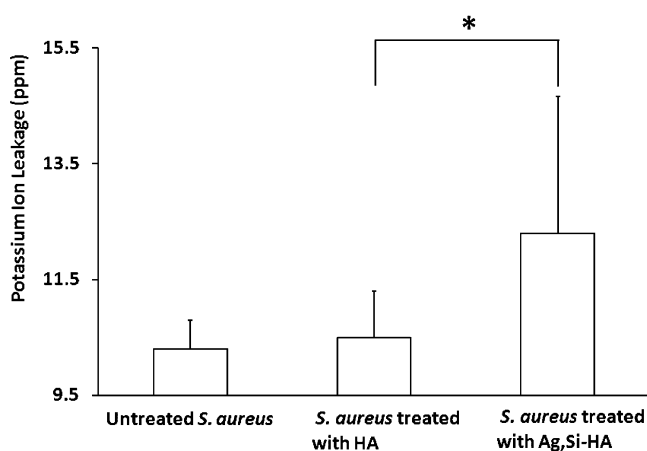

Figure 8. Amount of leakage of potassium ions from untreated *S. aureus* and *S. aureus* treated with HA and Ag,Si-HA after culturing for 6 h (bars represent standard error of the mean, * $p < 0.05$).

Figure 9. Cell proliferation of hASCs on HA, Ag-HA, Si-HA, and Ag,Si-HA at different time points. Bars represent standard error of the mean. [a] $p < 0.05$ for HA between groups; [b] $p < 0.05$ for Ag-HA between groups; [c] $p < 0.05$ for Si-HA between groups; [d] $p < 0.05$ for Ag,Si-HA between groups; [e] $p < 0.05$ when comparing Ag,Si-HA to HA within groups; [f] $p < 0.05$ when comparing Ag,Si-HA to Si-HA within groups.
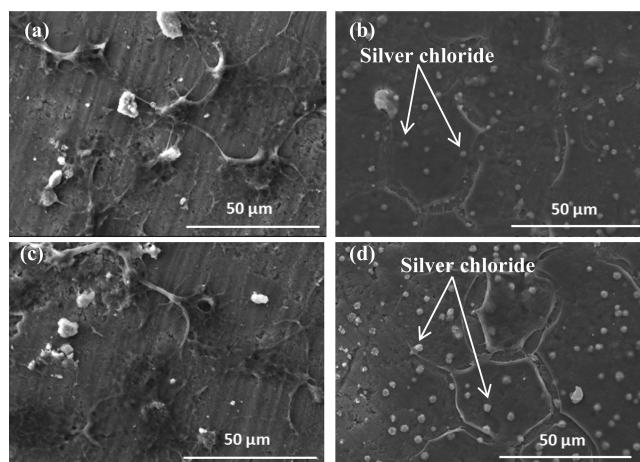
Figure 10. SEM images of hASCs cultured on (a) HA, (b) Ag-HA, (c) Si-HA, and (d) Ag,Si-HA on day 5 (1000× magnification).

Figure 11. SEM images of hASCs cultured on (a) HA, (b) Ag-HA, (c) Si-HA, and (d) Ag,Si-HA on day 14 (3500× magnification).
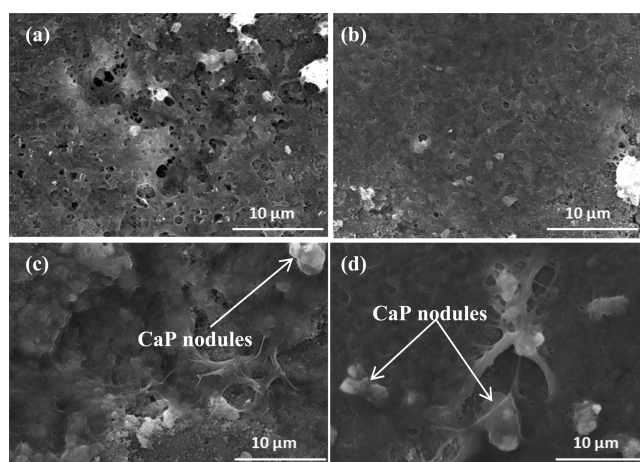
up to 21 days. On day 5, it was noticed that spherical agglomerates comprising silver and chlorine, as determined by energy dispersive X-ray spectroscopy spot analysis, were visible on the surface of AgHA and Ag,Si-HA (Figure 10b, d). This suggested that the presence of chloride ions in the culture medium was attracted to the surface-bound silver ions of Ag-HA and Ag,Si-HA, thus forming the spherical agglomerates.
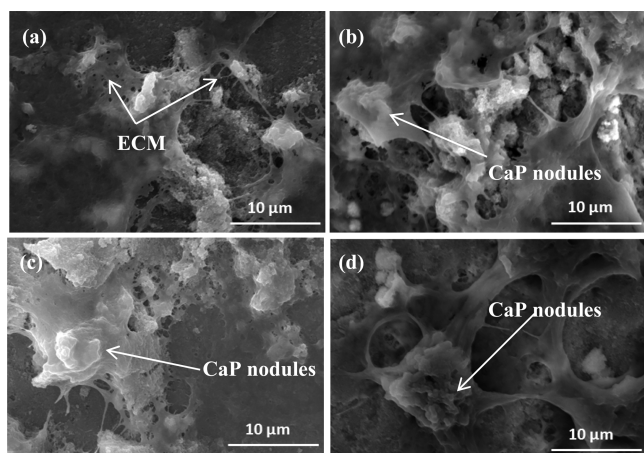
Figure 12. SEM images of hASCs cultured on (a) HA, (b) Ag-HA, (c) Si-HA, and (d) Ag,Si-HA on day 21 (3500× magnification).

On day 14, hASCs grew and multiplied, giving rise to more hASCs attaching and spreading across the surfaces of samples. Cells were seen adhering and spreading on top of each other, forming multilayer of cells with the production of extracellular matrix (ECM) on Ag,Si-HA and Si-HA (Figure 11). In addition, deposition of calcium phosphate minerals, as determined by energy dispersive X-ray spectroscopy spot analysis, was seen across the ECM surfaces for Si-HA and Ag,Si-HA on day 14, but this was not observed for HA and Ag-HA. On day 21, calcium phosphate mineral deposition was subsequently observed for HA and Ag-HA while numerous and larger mineral nodules were seen to distribute randomly on Si-HA and Ag,Si-HA (Figure 12).

The level of protein expression on HA and various substituted apatites is illustrated in Figure 13. First, a steady increase in the ALP activity at all time points was observed from hASCs cultured on HA, Ag-HA, Si-HA, and Ag,Si-HA (Figure 13a). When comparing among the samples, ALP activity of hASCs cultured on Si-HA was statistically the highest while the ALP activity of hASCs cultured on Ag-HA was the lowest on days 14, 21, and 28. It was noted that ALP activity of hASCs cultured on Ag,Si-HA was much higher ($p < 0.05$) than hASCs cultured on HA on days 14, 21, and 28. ALP production by hASCs cultured on Ag,Si-HA was ranked second among the substituted apatites.

An increasing production of the COL I expressed by hASCs cultured on HA, Ag-HA, Si-HA, and Ag,Si-HA from days 14 to 28 (Figure 13b) was noted. COL I produced by hASCs cultured on Ag,Si-HA was lower than the COL I expressed by hASCs cultured on Si-HA. Nevertheless, hASCs cultured on Ag,Si-HA expressed a greater amount of COL I than hASCs cultured on HA and Ag-HA on days 14 and 21. Overall, hASCs cultured on Ag,Si-HA produced the second highest amount of COL I expression as compared to those cultured on HA and substituted apatites. As COL I is an early differentiation marker of bone formation, its expression tends to reduce with time,[22] as demonstrated by the decrease in COL I expression on all samples on day 28.

Lastly, OCN expression was detected for hASCs cultured on all samples from day 14 onward and increased significantly with culturing period (Figure 13c). Similar to ALP and COL I expression, it was also observed that hASCs cultured on Ag,Si-HA expressed the second highest amount of OCN among HA and the substituted apatites.
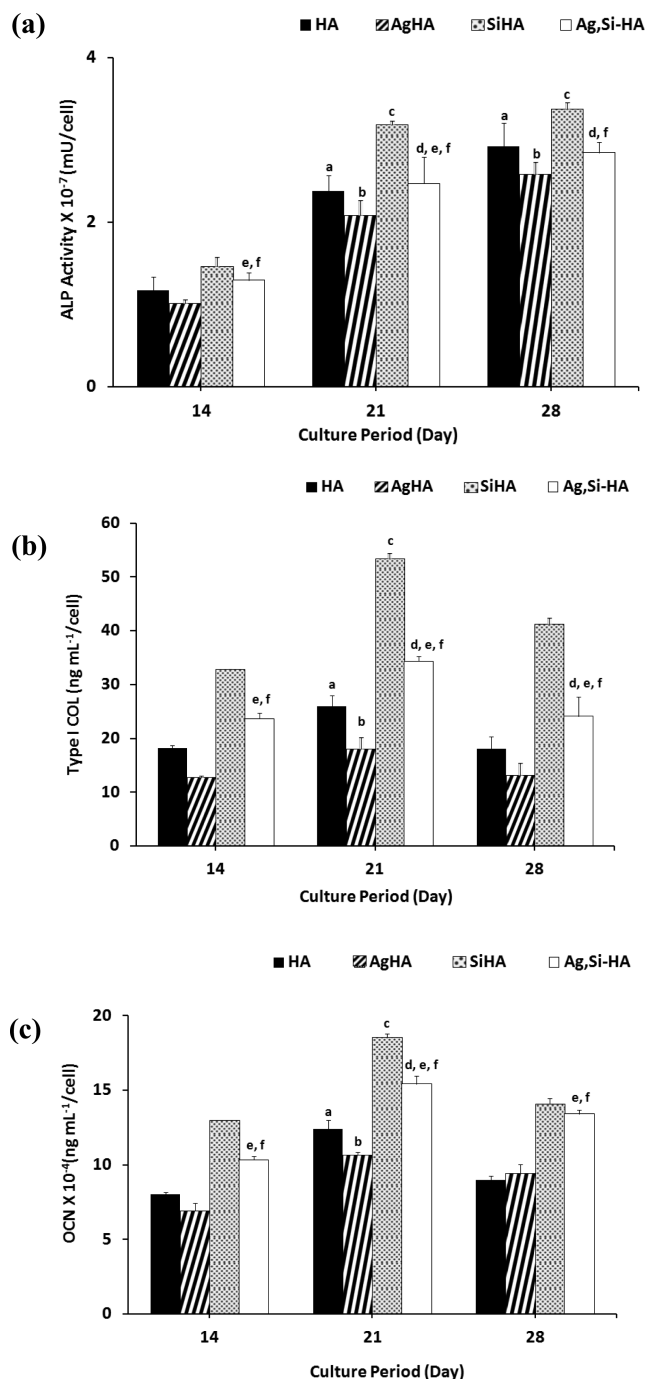
Figure 13. Quantitative measurement of protein expression on HA, Ag-HA, Si-HA, and Ag,Si-HA. Bars represent standard error of the mean. [a] $p < 0.05$ for HA between groups; [b] $p < 0.05$ for Ag-HA between groups; [c] $p < 0.05$ for Si-HA between groups; [d] $p < 0.05$ for Ag,Si-HA between groups; [e] $p < 0.05$ when comparing Ag,Si-HA to HA within groups; [f] $p < 0.05$ when comparing Ag,Si-HA to Ag-HA within groups.

4. DISCUSSION

Effective inhibition of bacterial adhesion at 6 h post-implantation is often regarded as the most critical period in preventing implant-related infection.[23] Over the period of 6 h, the implant is particularly susceptible to surface bacterial colonization, and beyond 6 h, adherent bacteria can proceed to form biofilm at the implant-tissue interface. This was observed in HA and Si-HA, whereby the growth of *S. aureus* reached a
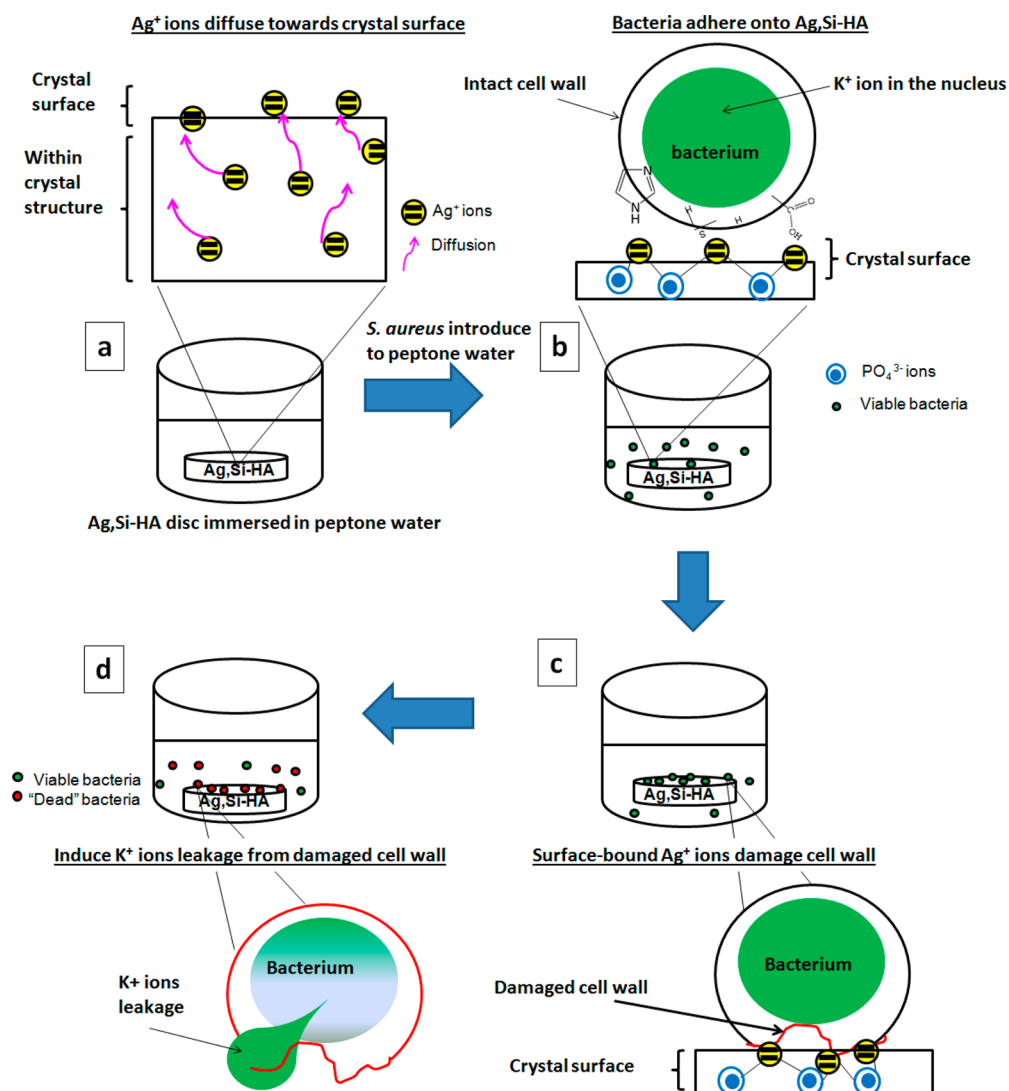
Figure 14. Schematic drawing of the proposed mechanism of antibacterial action of Ag,Si-HA. (a) Silver ions diffuse toward the surface of Ag,Si-HA, (b) bacteria adhere onto Ag,Si-HA, and (c) surface-bound silver ions of Ag,Si-HA damage the cell wall, and (d) induce potassium ions leakage from the damaged cell wall.

peak population of approximately 10^7 CFU/mL while obvious inhibition of bacterial growth on Ag-HA and Ag,Si-HA could be observed from 6 h onward (Figure 4).

Subsequently, the adherent *S. aureus* on Ag-HA and Ag,Si-HA was further reduced to zero at 18 h, and no viable adherent *S. aureus* was observed up to 168 h. Indeed, the inhibition of the adherent bacteria growth on Ag-HA and Ag,Si-HA was evident. Hence, the incorporation of silver in the apatite was effective in the prevention of bacteria adhesion on the surfaces of the implant. It was also interesting to note that the inhibition rates of adherent *S. aureus* between Ag,Si-HA and Ag-HA were similar. This phenomenon indicated that the incorporation of silicon into Ag-HA did not affect its antibacterial property.

Several authors[7,24,25] attributed the antibacterial action of Ag-HA to the release of silver ions from Ag-HA into the test solution. These Ag-HA were formed by adding the silver precursor with apatite (AgHA-IE). Ag-HA could also be formed by adding the silver precursor during the nucleation of apatite (AgHA-CP). Oh et al.[3] demonstrated that AgHA-CP containing 0.53 wt % silver had a more durable antibacterial effect than AgHA-IE containing 1.5 wt % silver content, despite

detecting a lower amount of released silver ions in the test medium. In addition, Stanic et al.[4] observed an effective antibacterial effect in AgHA-CP with negligible released silver ions. In this study, the growth of *S. aureus* in the test solution of the Ag,Si-HA disc on the inset (Figure 5) demonstrated indirect evidence that released silver ions did not provide effective antibacterial action. All these findings implied that AgHA-CP might not rely on the release of silver ions for its antibacterial action. In our recent study, the antibacterial action of AgHA-CP was investigated and reported to be dependent on its surface-bound silver ions.[8] Thus, the antibacterial action of the surface-bound silver ions of Ag,Si-HA was proposed through a mechanism as illustrated in Figure 14.

The mechanism of the antibacterial action for Ag,Si-HA was proposed in the following four steps. Step 1: silver ions diffused toward the crystal surface of Ag,Si-HA when immersed in solution (Figure 14a). XPS results demonstrated the presence of the silver ion (Ag^+) and metallic silver (Ag^0) on the surface of Ag,Si-HA, and this amount increased with the immersion period, indicating that silver ions (Ag^+) and metallic silver (Ag^0) diffused toward the crystal surface. As illustrated in

Figure 2, silver ions (Ag$^+$) fit the peaks in greater area; thus, there was a greater amount of silver ions (Ag$^+$) than metallic silver (Ag^0) on the surface. Hence, the antibacterial effect was contributed mainly by silver ions (Ag$^+$). Moreover, there was a minimal amount of released silver ions detected in the test solution, which further implied that silver ions remained bound to the crystal surface of Ag,Si-HA. Hence, local cytotoxicity of released silver ions at the implant site could be minimized as antibacterial action took place when surface-bound silver ions interacted with the adherent bacteria. In addition, the antibacterial efficiency of Ag,Si-HA could be maintained for a longer period of time.

Following on, Step 2: bacteria adhered onto Ag,Si-HA (Figure 14b). The cell envelope protein and enzymes of bacteria contain imidazole, amino, carboxyl, and thiol groups. These functional groups were electrostatically attracted to the surface-bound silver ions of Ag,Si-HA to undergo ion exchange.[26,27] Adhesion of bacteria onto the surface of Ag,Si-HA was observed in our previous study.[14]

As a result, Step 3: through ion exchange between the functional groups and the surface-bound silver of Ag,Si-HA, the cell wall of the bacteria was damaged (Figure 14c), and Step 4: potassium ions leakage was induced from the damaged cell wall, causing an increase in the permeability of cell membrane (Figure 14d). Gram staining results indicated the first sign of damage at the bacteria membrane of *S. aureus* treated with Ag,Si-HA. The reduced peptidoglycan layer of the cell wall was not able to retain the purple stain and was counterstained pink. By further examining the morphology changes at the cell wall, the separation of the cell membrane from the cell wall was observed. This resulted in osmotic pressure differences, thus rupturing the cell wall and inducing the potassium ion leakage.

The entry of noxious compounds was prevented by the cell membrane of the bacteria that served as a permeability barrier. With the increased permeability of the cell membrane, the defense system of the bacterium would be weakened, making the bacterium susceptible to the attack of the antibacterial agents, and thus resulting in cell death. Furthermore, a bacterium of disorganized shape and increased permeability of the cell membrane impaired the bacterium to regulate through the cytoplasmic membrane, losing its replication ability.[28] Similar to titanium dioxide,[29] silver-bound silver ions of Ag,Si-HA damaged the functional groups of the cell envelope, which in turn distorted the shape of the bacteria and increased permeability of the cell membrane. Thus, it was suggested that *S. aureus* treated with Ag,Si-HA underwent lysis, which explained the absence of viable adherent bacteria on Ag,Si-HA until 168 h. On a side note, there might be a possibility that the surface-bound silver ions might have invaded into the nucleus of the bacterium after damaging the cell wall. However, this requires further investigation. On the whole, this simple experiment demonstrated and validated the hypothesis that Ag,Si-HA synthesized by incorporating silver ions during the nucleation of apatite relied on the surface-bound silver ions for its antibacterial action. Silver ions were incorporated into the apatite structure and subsequently got diffused toward the surface crystal, whereby it could then exhibit oligodynamic effect to create toxicity on the bacteria. Thus, this created a complementary effect.

The in vitro study compared the biological responses of hASCs cultured on HA, Ag-HA, and Si-HA with Ag,Si-HA (Figures 9−13). Results demonstrated increasing growth activity and typical osteoblastic morphology for hASCs cultured

on HA, Ag-HA, Si-HA, and Ag,Si-HA. Thus, the incorporation of silver in HA did not affect the overall biocompatibility, and it was clear that 0.5 wt % silver did not induce any noticeable cytotoxicity effect.

Interestingly, silver chloride agglomerates were observed on Ag-HA and Ag,Si-HA in the field emission SEM micrographs (Figure 10b, d). This was due to the reaction between surface-bound silver ions of Ag,Si-HA and the free chloride ions in the culture medium. This phenomenon occurred as there were silver ions bound on the surface of Ag,Si-HA, which affirmed the hypothesis that silver ions in the crystal structure of Ag,Si-HA diffused toward the crystal surface. However, there is no implication on the silver chloride agglomerates formed on Ag-HA and Ag,Si-HA as the agglomerates do not affect the attachment of cells during bone regeneration. Furthermore, these agglomerates on Ag-HA and Ag,Si-HA seemed to be reduced from day 14 onward (Figure 11). The agglomerates might have dissolved into the culture medium with increasing culturing period.

The differentiation of hASCs on HA and substituted apatites was supported by the protein expression measurements (Figure 13). The production of ALP, COL I, and OCN from hASCs cultured on AgHA over 28 days were lower than hASCs cultured on HA. Similarly, the production of ALP, COL I, and OCN by hASCs cultured on Ag,Si-HA over 28 days was also lower than hASCs cultured on Si-HA. The reduced protein expression of hASCs cultured on Ag-HA and Ag,Si-HA could be attributed to the presence of silver. Although 0.5 wt % silver was demonstrated to exhibit an absence of cytotoxicity (Figure 9), the differentiation and biomineralization of hASCs were shown to be affected (Figure 13). This effect was also observed in metal ions such as the aluminum ion, which suppressed the expression of ALP and OCN at noncytotoxicity level.[30]

Nevertheless, with the incorporation of silicon into Ag-HA, the production of ALP, COL I, and OCN from hASCs cultured on Ag,Si-HA over 28 days greatly increased and even surpassed the amount that was produced by hASCs cultured on Ag-HA and HA. These results highlighted that the incorporation of silicon in Ag,Si-HA helped to mitigate the reduced cell differentiation caused by silver. Hence, all these results clearly demonstrated that silicon played an important role in promoting the differentiation and maturation of hASCs.

On the whole, this study demonstrates that Ag,Si-HA possesses a sustained antibacterial property without compromising its osteogenic property. Thus, it is a potential biomaterial in facilitating bone regeneration, with reduced bacterial infection, and is applicable for clinical applications such as infected sites in craniomaxillofacial and musculoskeletal defects.

5. CONCLUSIONS

Results demonstrated that surface-bound silver ions were shown to exert the antibacterial action, which resulted in the 7-log reduction of the adherent *S. aureus* bacteria on Ag,Si-HA and Ag-HA as compared to HA and Si-HA at 168 h. The antibacterial action of Ag,Si-HA was demonstrated through a four-step mechanism. Silver ions in the crystal structure diffused toward the crystal surface of Ag,Si-HA (Step 1). This was shown by the increasing silver content on the surface of Ag,Si-HA with the immersion period. Next, bacteria adhered on the Ag,Si-HA due to the electrostatic attraction between the protein and enzymes of the bacteria cell wall and the surface-bound silver of Ag,Si-HA (Step 2). Consequently, surface-

bound silver damaged the cell wall of the bacteria (Step 3) and thereby induced the leakage of cellular content of potassium ions (Step 4). Detachment of the cytoplasm membrane of bacteria and the reduction of the peptidoglycan layer of the cell wall of *S. aureus* treated with Ag,Si-HA was observed in the TEM micrographs and Gram staining, respectively. Furthermore, a greater amount of potassium content was measured in the test solution of Ag,Si-HA as compared to HA. All these results suggested the lysis of *S. aureus* having treated with Ag,Si-HA. Results of the in vitro cellular studies demonstrated typical osteoblastic morphology and increasing growth activity of hASCs cultured on HA, Ag-HA, Si-HA, and Ag,Si-HA. However, the incorporation of 0.5 wt % silver in apatite tended to reduce the bone differentiation of hASCs, and this was mitigated with the addition of 0.7 wt % silicon. Elevated levels of ALP, COL I, and OCN were expressed by hASCs on Ag,Si-HA as compared to HA and Ag-HA.

■ AUTHOR INFORMATION

Corresponding Author
*Phone: +65 6516 5233; fax: +65 6779 1459; e-mail: mpetes@ nus.edu.sg.

Notes
The content is solely the responsibility of the authors and does not necessarily represent the official views of the Ministry of Education (Singapore).
The authors declare no competing financial interest.

■ REFERENCES

(1) Darouiche, R. O. Treatment of Infections Associated with Surgical Implants. *N. Engl. J. Med.* **2004**, *350*, 1422−1429.

(2) Klasen, H. J. Historical Review of the Use of Silver in the Treatment of Burns. I. Early Uses. *Burns* **2000**, *26*, 117−130.

(3) Oh, K. S.; Park, S. H.; Jeong, Y. K. Durability in Antimicrobial Effects of Silver Doped Hydroxyapatite Depending on the Synthesis Route. *Mater. Sci. Forum* **2004**, *449−452*, 1233−1236.

(4) Stanic, V.; Janackovic, D.; Dimitrijevic, S.; Tanaskovic, S. B.; Mitric, M.; Pavlovic, M. S.; Krstic, A.; Jovanovic, D.; Raicevic, S. Synthesis of Antimicrobial Monophase Silver-Doped Hydroxyapatite Nanopowders for Bone Tissue Engineering. *Appl. Surf. Sci.* **2011**, *257*, 4510−4518.

(5) Ando, Y.; Miyamoto, H.; Noda, I.; Sakurai, N.; Akiyama, T.; Yonekura, Y.; Shimazaki, T.; Miyazaki, M.; Mawatari, M.; Hotokebuchi, T. Calcium Phosphate Coating Containing Silver Shows High Antibacterial Activity and Low Cytotoxicity and Inhibits Bacterial Adhesion. *Mater. Sci. Eng., C* **2010**, *30*, 175−180.

(6) Rameshbabu, N.; Kumar, T. S. S.; Prabhakar, T. G.; Sastry, V. S.; Murty, K. V. G. K.; Rao, K. P. Antibacterial Nanosized Silver Substituted Hydroxyapatite: Synthesis and Characterization. *J. Biomed. Mater. Res.* **2007**, *80A*, 581−591.

(7) Kim, T. N.; Feng, Q. L.; Kim, J. O.; Wu, J.; Wang, H.; Chen, G. C.; Cui, F. Z. Antimicrobial Effects of Metal Ions (Ag^+, Cu^{2+}, Zn^{2+}) in Hydroxyapatite. *J. Mater. Sci.: Mater. Med.* **1998**, *9*, 129−134.

(8) Lim, P. N.; Teo, E. Y.; Ho, B.; Tay, B. Y.; Thian, E. S. Effect of Silver Content on the Antibacterial and Bioactive Properties of Silver-Substituted Hydroxyapatite. *J. Biomed. Mater. Res.* **2013**, *101A*, 2456−2464.

(9) Chen, Y.; Zheng, X.; Xie, Y.; Ding, C.; Ruan, H.; Fan, C. Anti-Bacterial and Cytotoxic Properties of Plasma Sprayed Silver-Containing HA Coatings. *J. Mater. Sci.: Mater. Med.* **2008**, *19*, 3603−3609.

(10) Porter, A. E.; Best, S. M.; Bonfield, W. Ultrastructural Comparison of Hydroxyapatite and Silicon-Substituted Hydroxyapatite for Biomedical Applications. *J. Biomed. Mater. Res.* **2004**, *68A*, 133−141.

(11) Porter, A. E.; Patel, N.; Skepper, J. N.; Best, S. M.; Bonfield, W. Comparison of *in Vivo* Dissolution Processes in Hydroxyapatite and Silicon-Substituted Hydroxyapatite Bioceramics. *Biomaterials* **2003**, *24*, 4609−4620.

(12) Balas, F.; Pérez-Pariente, J.; Vallet-Regí, M. *In Vitro* Bioactivity of Silicon-Substituted Hydroxyapatites. *J. Biomed. Mater. Res.* **2003**, *66A*, 364−375.

(13) Patel, N.; Best, S. M.; Bonfield, W.; Gibson, I. R.; Hing, K. A.; Damien, E.; Revell, P. A. A Comparative Study on the *in Vivo* Behavior of Hydroxyapatite and Silicon Substituted Hydroxyapatite Granules. *J. Mater. Sci.: Mater. Med.* **2002**, *13*, 1199−1206.

(14) Lim, P. N.; Shi, Z. L.; Neoh, K. G.; Ho, B.; Tay, B. Y.; Thian, E. S. The Effects of Silver, Silicon-Containing Apatite Towards Bacteria and Cell Responses. *Biomed. Mater.* **2013**, *9*, 015010.

(15) Lim, P. N.; Tay, B. Y.; Chan, C. M.; Thian, E. S. Synthesis and Characterization of Silver/Silicon-Cosubstituted Nanohydroxyapatite. *J. Biomed. Mater. Res.* **2012**, *100B*, 285−291.

(16) Hing, K. A.; Revell, P. A.; Smith, N.; Buckland, T. Effect of Silicon Level on Rate, Quality and Progression of Bone Healing within Silicate-Substituted Porous Hydroxyapatite Scaffolds. *Biomaterials* **2006**, *27*, 5014−5026.

(17) Lim, P. N.; Chang, L.; Ho, B.; Tay, B. Y.; Choong, C.; Thian, E. S. Development of New Generation Bone Graft Material: Silicon and Silver Co-Substituted Apatite with Bi-Functional Properties. *MRS Online Proc. Libr.* **2014**, DOI: 10.1557/opl.2014.44.

(18) Gastaldi, G.; Asti, A.; Scaffino, M. F.; Visai, L.; Saino, E.; Cometa, A. M.; Benazzo, F. Human Adipose-Derived Stem Cells (hASCs) Proliferate and Differentiate in Osteoblast-like Cells on Trabecular Titanium Scaffolds. *J. Biomed. Mater. Res.* **2010**, *94A*, 790−799.

(19) MyAssay. Online Data Analysis. Online. 2013. http://www.myassays.com/four-parameter-logistic-curve.assay (Accessed on December 14, 2013.

(20) *XPS and Auger Handbook*, Document number 600001, issue 2; Thermo VG-Scientific: Waltham, MA, 2003.

(21) Saito, T.; Iwase, T.; Horie, J.; Morioka, T. Mode of Photocatalytic Bactericidal Action of Powdered Semiconductor TiO_2 on *Mutans Streptococci*. *J. Photochem. Photobiol., B* **1992**, *14*, 369−379.

(22) Donahue, H. J.; Li, Z.; Zhou, Z.; Yellowley, C. E. Differentiation of Human Fetal Osteoblastic Cells and Gap Junctional Intercellular Communication. *Am. J. Physiol.: Cell Physiol.* **2000**, *278*, C315−C322.

(23) Poelstra, K. A.; Barekzi, N. A.; Rediske, A. M.; Felts, A. G.; Slunt, J. B.; Grainger, D. W. Prophylactic Treatment of Gram-Positive and Gram-Negative Abdominal Implant Infections Using Locally Delivered Polyclonal Antibodies. *J. Biomed. Mater. Res.* **2002**, *60A*, 206−215.

(24) Wu, X.; Li, J.; Wang, L.; Huang, D.; Zuo, Y.; Li, Y. The Release Properties of Silver Ions from Ag-nHA/TiO_2/PA66 Antimicrobial Composite Scaffolds. *Biomed. Mater.* **2010**, *5*, 044105.

(25) Chen, Y.; Zheng, X.; Xie, Y.; Ji, H.; Ding, C.; Li, H.; Dai, K. Silver Release from Silver-Containing Hydroxyapatite Coatings. *Surf. Coat. Technol.* **2010**, *205*, 1892−1896.

(26) Holt, K. B.; Bard, A. J. Interaction of Silver(I) Ions with the Respiratory Chain of *Escherichia coli*: An Electrochemical and Scanning Electrochemical Microscopy Study of the Antimicrobial Mechanism of Micromolar Ag^+. *Biochemistry* **2005**, *44*, 13214−12223.

(27) Liau, S. Y.; Read, D. C.; Pugh, W. J.; Furr, J. R.; Russell, A. D. Interaction of Silver Nitrate with Readily Identifiable Groups: Relationship to the Antibacterial Action of Silver Ions. *Lett. Appl. Microbiol.* **1997**, *25*, 279−283.

(28) Li, K.; Xie, Y.; Huang, L.; Ji, H.; Zheng, X. Antibacterial Mechanism of Plasma Sprayed $Ca_2ZnSi_2O_7$ Coating against *Escherichia coli*. *J. Mater. Sci.: Mater. Med.* **2014**, *24*, 171−178.

(29) Nadtochenkoa, V. A.; Rinconb, A. G.; Stancaa, S. E.; Kiwi, J. Dynamics of *E. coli* Membrane Cell Peroxidation During TiO_2 Photocatalysis Studied by ATR-FTIR Spectroscopy and AFM Microscopy. *J. Photochem. Photobiol., A* **2005**, *169*, 131−137.

(30) Sun, Z. L.; Wataha, J. C.; Hanks, C. T. Effects of Metal Ions on Osteoblast-like Cell Metabolism and Differentiation. *J. Biomed. Mater. Res.* **1997**, *34A*, 29−37.

17092

dx.doi.org/10.1021/am504716g | *ACS Appl. Mater. Interfaces* 2014, 6, 17082−17092